Laboratory results for speckle suppression with a self-coherent camera.

Pierre Baudoz[1a], Marion Mas[1], Raphael Galicher[2,3], Gerard Rousset[1], and Johan Mazoyer[1]

[1] LESIA, Observatoire de Paris, CNRS, Université Pierre et Marie Curie Paris 6 and Université Denis Diderot Paris7 – 5, place Jules Janssen, 92195 Meudon, France.
[2] National Research Council Canada, Herzberg Institute of Astrophysics, 5071 West Saanich Road, Victoria, BC, V9E 2E7, Canada
[3] Dept. de Physique, Université de Montréal, C.P. 6128 Succ. Centre-ville, Montréal, Qc, H3C 3J7, Canada

Abstract. Direct imaging is a powerful tool for exoplanet atmosphere characterization. High performance of these techniques requires extreme wavefront correction for ground-based instruments as well as space projects. Wavefront sensors are usually physically separated from the common optics by a beam splitter in classical AO system. This separation introduces differential aberrations that are not measured by the wavefront sensor, which limits the performance of a planet finder instrument. We propose to use the Self-Coherent Camera (SCC) to measure the aberrations directly in the final coronagraphic science focal plane. The SCC is based on the principle of light coherence and allows us to estimate the wavefront errors upstream the coronagraph by spatially encoding the speckles with fringes in the final image. After recalling the SCC principle, we will present laboratory results on speckle suppression and compare them with expected performances from numerical simulations.

1 Introduction

Understanding the formation, evolution and surprising diversity of exoplanetary systems is one of the few major challenges of current astrophysics. The international community has defined a long-term strategy based on both theoretical works and the study and development of dedicated facilities from the ground and from space. High contrast direct imaging has an important role to play in the completion of indirect detection techniques such as transits and radial velocities. Today, a few young planets at large separations have already been detected [1,2] and their characterization is starting. Ultimately, direct detection could allow us to fully characterize the properties of exoplanets, including indications of habitability and physics and chemistry of their atmosphere. The required contrast capability for exoplanet imaging is the main limitation to discoveries in this field. The first generation of ground-based instruments dedicated to high contrast imaging is currently being developed both in Europe and in North America by large international consortia [3,4]. These instruments are now close to starting operations, with a contrast performance $> 10^{-6}$ to 10^{-7} for detecting young Jupiter-like planets within 0.5 arcsec from their star, well inside the stellar halo.

A dramatic improvement of contrast performance is mandatory to study lower mass planets like Neptunes or possibly rocky planets. This is one of the key motivation for the future extremely large telescopes (ELT), the dominant infrastructures of tomorrow's optical and infrared astronomy. This dramatic improvement of exoplanet detection performance requires a deep understanding of the limitations for high contrast imaging and new technological solutions that can self-calibrate the observations. One solution proposed for the direct planet detection on ELT is the Self-Coherent Camera (SCC). The SCC is a concept of high contrast imaging instrument [5] that takes benefit from the coherence between the stellar leakage speckles and the stellar light rejected by a coronagraph. This property of coherence is used to measure the residual phase aberration [6] or detect a planet among the fringed speckles [5]. We will only describe the first capability in this paper. Preliminary simulation of the SCC performance on high contrast imaging instrument of the European ELT are promising [7]. However, at this stage of the development, a laboratory test to verify the capability of a real setup is mandatory.

[a] e-mail: pierre.baudoz@obspm.fr

In this paper, after recalling the principle of the SCC, we present how we estimate the phase from the SCC focal plane image in the case of a real coronagraph. After a brief description of the test bench, we present laboratory results and compare them to numerical simulations.

2 Principle of phase estimation in the Self-Coherent Camera

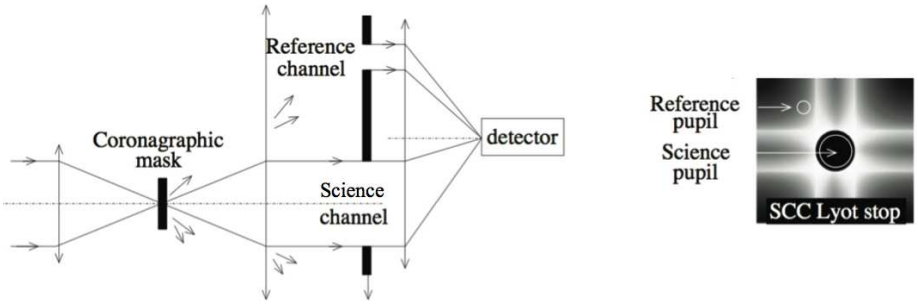

Fig. 1. Principle of the SCC coupled with a Four Quadrant Phase Mask (FQPM) coronagraph. The image on the right shows the light distribution in the pupil plane downstream the coronagraphic focal plane.

A robust design can associate the SCC with most of the coronagraphs by simply modifying the Lyot stop geometry [6]. The principle of the SCC coupled with a Four Quadrant Phase Mask (FQPM) coronagraph [8] is shown in Figure 1. As in the classical Lyot coronagraph, the star is focalized on a coronagraphic mask. In the pupil downstream of the focal plane mask, an unaberrated stellar light is fully diffracted outside of the pupil geometry [9]. The Lyot stop is modified to add a reference pupil (Figure 1, right). When the beam upstream the coronagraph is aberrated, there is residual light in the science pupil (classical Lyot stop) that can interfere with the reference pupil to create fringed speckles on the detector, which can be used to measure the phase aberrations. Performance of the SCC have already been assessed for space-based [10] as well as ground-based observation [7].

Below, we describe the formalism to estimate the phase using the Self-Coherent Camera coupled with a FQPM coronagraph.

Following the formalism given in Galicher et al. 2008 and 2010 [6, 10], we can write the monochromatic interferential image on the detector I:

$$I(\alpha) = |A_S(\alpha)|^2 + |A_R(\alpha)|^2 + A_S(\alpha)A_R(\alpha)^* \exp\left(\frac{2i\pi\alpha\xi_0}{\lambda_0}\right) + A_S(\alpha)^* A_R(\alpha) \exp\left(\frac{-2i\pi\alpha\xi_0}{\lambda_0}\right) \quad (1)$$

where $A_S(\alpha)$ and $A_R(\alpha)$ are the complex amplitudes in the focal plane that propagate through the science pupil and the reference pupil respectively. α is the focal plane angular coordinate, λ_0 is the wavelength considered and ξ_0 is the distance that separates the two pupils.

As already described in previous work [6, 10], we can extract the modulated part $I_-(\alpha)$ or $I_+(\alpha)$ of $I(\alpha)$ if $\xi_0 > \frac{3D_L}{2} + \frac{D_R}{2}$ with D_L the Lyot diameter and D_R the reference pupil diameter. To do it, we select one of the two lateral peaks of the inverse Fourier transform of I and apply a Fourier transform to it. The recentred I_- contains a combination of A_S and A_R and can be written:

$$I_-(\alpha) = A_S(\alpha)A_R(\alpha)^* \quad (2)$$

For monochromatic images, the complex amplitude downstream the coronagraph $\psi_S(u)$ (u is the pupil plane coordinate) can be described using I_-:

$$\psi_S(u) = F^{-1}\left[\frac{I_-(\alpha)}{A_R(\alpha)^*}\right](u) \quad (3)$$

With F^{-1} describing the inverse Fourier transform. We want to get back to the complex amplitude in the upstream pupil plane ψ'_S, which contains the phase aberrations we try to estimate. Usual propagation model trough coronagraph can give us the relation between the downstream complex amplitude ψ_S, the upstream complex amplitude ψ'_S, the coronagraphic focal plane mask function M, and the Lyot stop L.

$$\psi_S = \left(\psi'_S * F^{-1}(M)\right) L \tag{4}$$

where $*$ denotes the convolution. To simplify the equations, from now on, we drop both coordinates in the pupil and the focal plane. Assuming small phase ϕ and amplitude a defects, we can simplify the upstream complex amplitude ψ'_S

$$\psi'_S = P \exp(i\phi + a) \approx P + i\phi P + aP \tag{5}$$

Eq. 4 can be rewritten:

$$\psi_S = \left(P * F^{-1}(M)\right) L + \left(P(i\phi + a) * F^{-1}(M)\right) L \tag{6}$$

The first term is equal to zero for a coronagraph that can utterly suppress the field inside the pupil downstream the focal mask. This is the case of the FQPM coronagraph assuming an infinite field, perfect transitions, an unobstructed pupil, and monochromatic light [9].

Removing the first term and using the definition of ψ_S in Eq. 3, we write :

$$\left(P(i\phi + a) * F^{-1}(M)\right) L = F^{-1}\left[\frac{I_-}{A_R^*}\right] \tag{7}$$

Table 1. Equations used to calculate images shown in Figure 2.

Image 1	Image 2	Image 3	Image 4	Image 5
ϕP	$\phi P * F^{-1}(M)$	$\left(\phi P * F^{-1}(M)\right) P$	$\left\{\left[\left(\phi P * F^{-1}(M)\right) P\right] * F^{-1}(\frac{1}{M})\right\} P$	Image 1- Image 4

The convolution of ϕP (or aP) with a finite function will dilute the information outside P. As a consequence, even for L equal to P, ϕP (or aP) cannot be fully retrieved. However, for small inner working angle coronagraphs like the FQPM, we can expect that this convolution will be rather limited because the effect of such coronagraph are limited to the central part of the image. Thus, large and mid spatial frequencies should not be very affected. We simulate the case of the FQPM coronagraph to verify that. The results are shown in Figure 2. The five images are simulated following the equations described in Table 1.

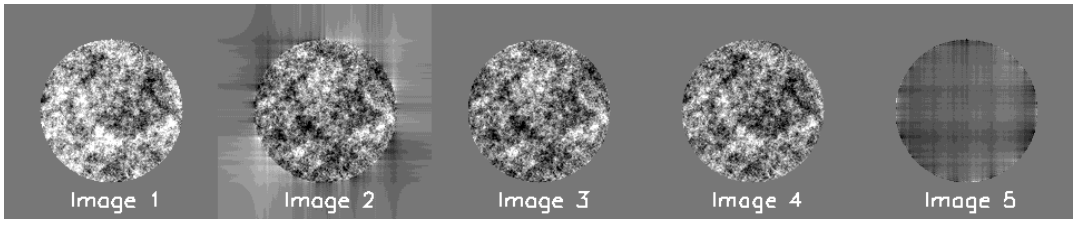

Fig. 2. Images calculated using equations given in Table 1 to compare the phase ϕ with its estimation by the SCC. Same linear scale for all images

On the left side (image 1), we show the simulated ϕP that is a random phase with a Power Spectral Density (PSD) in f^{-2}. On image 2, we show the distribution of the convolution between the phase and the Fourier transform of the coronagraphic mask before applying the Lyot stop here assumed to be equal to the pupil P. The filtering by the Lyot is applied on image 3. We can notice that the information removed in the filtering is rather small. On image 4, we try to apply a convolution by $F^{-1}\left(\frac{1}{M}\right)$ and a filtering by the pupil function since we are only interested by the information inside the pupil. Image 4 and 1 are very alike but the difference (image 5) shows diffraction effects certainly from the FQPM mask inside the pupil, especially around the edges. The root mean square (RMS) of the difference amounts to about 30 % of the RMS deviation of the phase ϕP. Even though this seems large, we decide to assume that this estimate is close enough to the phase for iteration to converge to the right phase. It was proved to be working with numerical simulation [10] and we show in Sect. 3.3 that it is also working on laboratory bench. Applying the same process of deconvolution and filtering by the phase to both terms of Eq. 7, we can rewrite Eq. 7:

$$\left\{\left[\left(i\phi P * F^{-1}(M)\right) P\right] * F^{-1}(\frac{1}{M})\right\} P + \left\{\left[\left(aP * F^{-1}(M)\right) P\right] * F^{-1}(\frac{1}{M})\right\} P = F^{-1}\left[\frac{I_-}{MA_R^*}\right] P \quad (8)$$

Note that we can divide by M only if M is never equal to zero (practically, this is the case for phase mask coronagraph). Note also that $F^{-1}(M)$ and $F^{-1}\left(\frac{1}{M}\right)$ are real because M is real and even in the case of the FQPM. Thus the real part (amplitude) and the imaginary part (phase) can be treated separately in Eq. 8. Assuming we are working with Lyot stop size close to the pupil one, we suppose that the left term of Eq. 8 is a good estimate of phase and amplitude defects, i.e. image 4 is almost equal to image 1. Thus we replace the left term of Eq. 8 by $i\phi_{estimate} + a_{estimate}$:

$$i\phi_{estimate} + a_{estimate} \approx F^{-1}\left[\frac{I_-}{MA_R^*}\right] P \quad (9)$$

Practically, the diameter of the reference pupil is much smaller than the Lyot stop. A_R is then much larger than the diffracted core from the Lyot stop. The angular frequencies that can be corrected by the deformable mirror (DM) are limited by its number of actuators. The amplitude A_R can be rather flat over these angular frequencies if the reference pupil is small enough. In this case, A_R is approximate to a constant and the wavefront estimation is:

$$i\phi_{estimate} + a_{estimate} \propto F^{-1}\left[\frac{I_-}{M}\right] P \quad (10)$$

Practically, we select one of the two lateral peaks of the inverse Fourier transform of I and apply a Fourier transform to it. The recentred I_- is then divided by a numerical mask M. We extract the imaginary part of the inverse Fourier transform of this function to get the estimated phase $\phi_{estimate}$ that will be used to calculate the voltage to be send to the DM for the phase correction. To avoid aliasing from high order phase defects in our phase estimation, we can also apply to I_- a filter that suppresses all frequencies larger than the cut-off frequency of the DM.

3 Laboratory tests

3.1 Test bench description

The test bench we are using to measure the SCC performance is described in details in Mas et al. 2010 [11]. The main components used for the tests described in this paper are:

1. An optical fiber source that is fed by a laser diode fiber (@ 625 nm)
2. A fully reflective optical design creating 3 pupil planes where we place:
   (a) An entrance pupil plane of 8.1 mm and a TT mirror
   (b) A Boston Micromachines deformable mirror (DM) of 32x32 actuators with a pitch of 0.3 mm

   (c) The Lyot stop of 8mm (99% filtering) and a reference pupil of 0.3 mm with ξ_0 = 13 mm
3. And 3 focal planes, two of which including:
   (a) A monochromatic Four Quadrant phase mask [8] optimized for 625 nm
   (b) A CCD camera of 640x480 pixels (400x400 used) with readout noise of 15 e- and a Full Well capacity of 13 000 e-
4. A set of Neutral Density filters to record PSF images (no coronagraph) and coronagraphic images
5. An additional lens that can be inserted in front of the camera for pupil plane imaging
6. A software (labview) that can control the DM using control matrix built as described below

To take into account all the effects of the laboratory setup and the effects of the approximations we took in the previous section, we record an interaction matrix by pulling one actuator at a time and record $\phi_{estimate}$ and $a_{estimate}$. To remove the phase and amplitude defects of the bench, the actual measurement is the difference between the estimations when pushing and pulling the actuator. Since the DM introduces only phase, $a_{estimate}$ will be null or almost for an optical path difference equal to zero between the science channel and the reference channel (Figure 1). Thus, we only use $\phi_{estimate}$ to build the interaction matrix. Example of $\phi_{estimate}$ for a few actuators are given in Figure 3. The cross is an artifact introduced by the convolution by M and $\frac{1}{M}$ of the actuator phase influence. The central core is an estimation of this phase. The actuators located on the edges are not very well estimated because of the coronagraph effect and the readout noise (Figure 3). To remove most of these effects (cross, noise, edge actuators badly estimated), we choose to create a synthetic interaction matrix using a gaussian function that fits the core of the image.

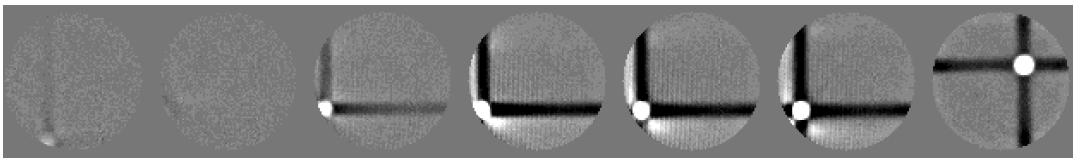

Fig. 3. Recorded estimation of the actuator phase influence. Same power law scale for all the actuators. The scale is stretched to show effects of actuators at the edge of the pupil. The dark cross is about 10 times fainter than the central core for central actuators.

First, the geometry (pitch, orientation) of the actuator grid is measured on the $\phi_{estimate}$ of the 10x10 most central actuators. On the same actuators, we measure the median width in both direction and the amplitude of the central core with a gaussian fitting algorithm. A synthetic grid of actuators using these values is then created to simulate our synthetic interaction matrix. We remove the edge actuators from the matrix when they have a low impact on the pupil phase.

The generalized inverse of the matrix is calculated using a Singular Value Decomposition algorithm and removing the lowest singular values. The control matrix obtained can be multiplied by the vector measuring $\phi_{estimate}$ to calculate the set of voltages to send to the DM. We use a simple integrator control low with a relatively low gain ($g < 0.4$). Note that the gain is proportional to the total flux of the source [6]. As the aberrations are corrected, the coronagraph performance is getting better and the speckles are getting fainter. Since we correct the residuals on several order of magnitudes, we have to increase the source flux to minimize the readout noise limitation and decrease the control gain accordingly.

3.2 Estimation of bench defects

First, let's estimate the aberrations on our bench before correction with the DM. These aberrations include the errors introduced by the DM. We flattened the DM using a commercial Shack-Hartmann wavefront sensor using a 32x32 lenslet array. The absolute precision of the instrument is given to 10 nm but we had to introduce a dedicated optical arm to image the pupil on the sensor. Defects on this arm have been calibrated using a point source and we expect a precision of the order of 20 nm over

the frequency measured by the sensor. We show in Figure 4 (right), the average radial profile for the PSF intensity (without coronagraph) compared to the average radial profile for the image with the sole coronagraph (no reference pupil). The image corresponding to this last profile is shown in Figure 5 (upper left image).

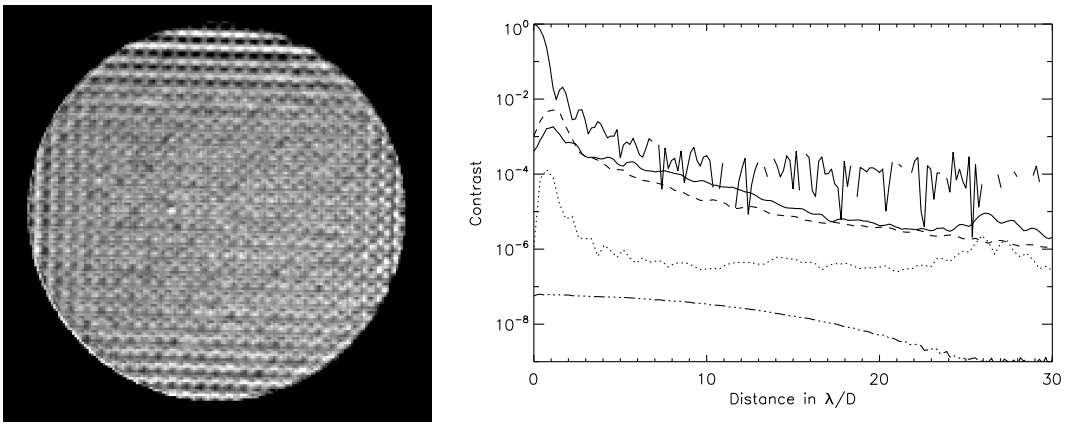

Fig. 4. Left: Pupil illumination measured on the test bench. Right: Average radial profiles of PSF (solid, up), coronagraphic image (solid, bottom), numerically simulated coronagraphic images using phase (dashed) or amplitude (dotted), and reference image (dashed-dotted).

We compared this profile with several simulated profiles of FQPM images obtained with different phase assumptions. A rather good fit is shown in Figure 4 (right, dashed line) and is drawn for a phase of 0.3 rad RMS (corresponding to 30 nm RMS) and a PSD of this phase in $f^{-2.5}$. The low frequency is a little overestimated between 1 and 2 λ/D and underestimated until 16 λ/D. But for the spatial frequency below 13.5 λ/D (cut-off frequency of the DM for this test), this may come from the way we flattened the DM. Indeed, the DM has been flattened directly on the test bench so it certainly corrected part of the bench lowest frequencies that we took good care to correct. Since the positioning of the DM with respect to the sensor was noisy, it may have induce DM flat errors in the spatial frequency between 2 and 13.5 λ/D. A peak in the radial profile also appears for spatial frequency around 26-27 λ/D which corresponds to twice the cut-off frequency of the DM correction. It corresponds to small scale structure with a typical size equal to the actuator pitch. As shown on the upper left image in Figure 5, theses defects are localized on the images and are well known features for this DM [12].

We can also estimate the variance of the amplitude defects using an image of the pupil illumination recorded on the bench (Figure 4, left). From this image, the level of the amplitude defects is estimated at about 10% RMS in intensity. Sub-actuator structures clearly appear, as well as a low spatial frequency effect coming from the actuators on the edges of the DM. Introducing these estimated amplitude in our simulation can help us take them into account. It sets the level of the residual speckles if all the phase was corrected. We notice that its level at twice the cut-off frequency does not reach the residual level of the coronagraphic image. The sub-actuator structures must also affects the phase but can not be measured on the pupil illumination and the spatial resolution of $\phi_{estimate}$ is not good enough to measure them with our setup. In Figure 4, we also plot the average radial profile of the reference image normalized to the PSF image ($|A_R|^2$). Its contribution to the SCC image I is negligible unless correction level reaches 10^{-7} or lower. Its relative flatness over the corrected area (13.5x13.5 λ/D) is in agreement with our approximation of a constant A_R that led us from Eq. 9 to Eq. 10.

3.3 Laboratory results after correction using phase and amplitude estimated by the SCC

The correction is applied on the DM as described in Sect. 3.1. The correction converges in a few iterations to a readout noise limited image. We need to increase the source flux, decrease the gain

accordingly and restart the correction a few times until we reach a constant residual speckles distribution. This final image is shown in Figure 5 (top centered image) and the average radial profile is given in Figure 6 (left, solid line) and compared to the case with no correction (left, dashed line). The DM helps to decrease by a factor 100 at least the level of the coronagraphic image between 2 and 10 λ/D and the mean speckle level is below 3.10^{-6} between 4 and 12 λ/D.

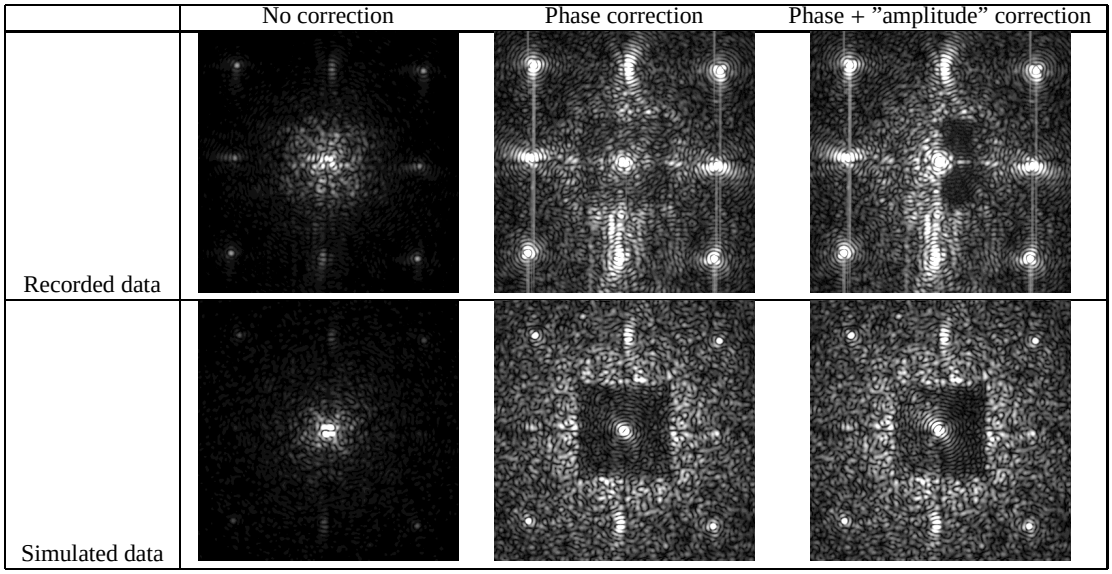

Fig. 5. Comparison between recorded and simulated data without correction, with correction of phase, and with correction taking into account phase and amplitude. The scale is a power law and the same for all images but uncorrected image have been divided by 100 to reach the same range level than the corrected images.

We notice that the level of the image after the cut-off frequency is improved by the correction even if we specifically remove these frequencies from the phase estimation (Eq. 10). This is certainly coming from the fact that sub-actuator structures vary when correcting and these structures have an effect at these frequencies and certainly both in phase and amplitude. At the position of twice the DM frequency cut-off, the level also seems to improve but this is an artifact coming from the fact that diffracted structures saturate the detector (see images in Figure 5). We also draw on this figure the simulated correction assuming the same amplitude and phase as in Sect. 3.2 but with all the frequencies reachable by the DM set to zero in the phase PSD. We notice that the level reached is higher than expected in the correction area and lower in the external area. It may be an underestimation of the amplitude error which should dominate in the correction area and an overestimation of the phase outside of this area. This also visible when comparing simulated and recorded images in Figure 5.

Since amplitude defects may set the limitation inside the correction area, we choose to correct for them in half the field. We use both phase and amplitude estimates given by Eq. 10 and apply the technique proposed by Borde & Traub 2006 [13] to estimate the voltage to send to the DM and correct for both defects in half the field (top right image in Figure 5). We calculate the average radial profile only on the corrected side (right side) and plot it in Figure 6 right (solid line). The residual speckles gets lower than 4.10^{-7} between 4 and 12 λ/D. We also compare the data to numerical simulation using the same hypotheses than previously. The level reached is close to the one simulated except for uncorrected frequencies where the phase level is overestimated. The underestimation of the amplitude does not appear on the radial profile but clearly appears when comparing simulated and recorded images: the left level of the lower right image in Figure 5 is much fainter than the one effectively recorded. Increasing the amplitude defects inside the correction would better explain the recorded

image for both sole phase and phase+amplitude corrections. Besides, it could also explain the limited level of residual light reached when correcting phase errors only on the full correction area.

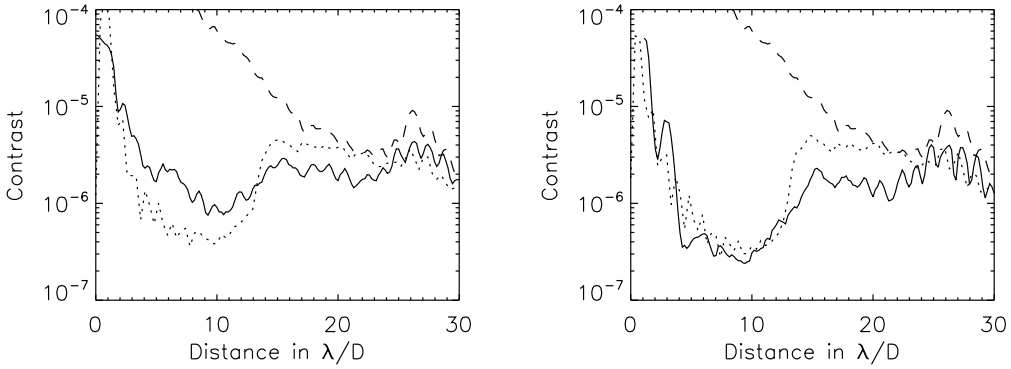

Fig. 6. Left: Average radial profile for recorded uncorrected image (dashed), recorded phase corrected data (solid), simulated phase corrected data (dotted). Right: Average radial profile for recorded uncorrected image (dashed), recorded phase+amplitude corrected data (solid), simulated phase+amplitude corrected data (dotted).

4 Conclusion

We demonstrated that the concept of Self-Coherent Camera coupled with a Four Quadrant Phase mask coronagraph is working in laboratory environment with monochromatic source. The simple linear phase estimation we use is enough to reach correction well in agreement with the simulation. When correcting phase over the full correction area of the DM (13.5x13.5 λ/D), the level of residual light is below 3.10^{-6} between 4 and 12 λ/D mostly limited by amplitude errors. When correcting for phase and amplitude errors in half the field, the level of the residual speckles gets lower than 4.10^{-7} between 4 and 12 λ/D. Improvements can be obtained when using more optimized correction algorithm that minimize the light inside the correction area instead of minimizing the phase in the pupil as presented in this paper. This will be presented in a forthcoming paper. Chromatic tests must also be performed to estimate more precisely the overall performance of such an instrument on a telescope.

References

1. Marois, C. et al., *Science*, **322**, (2008) 1348
2. Lagrange, A.-M., et al., *Astronomy and Astrophysics*, **493**, (2009) L21
3. Beuzit, J.-L., et al., *SPIE*, **7014** (2008) 701418
4. Macintosh, B., et al., *SPIE*, **7015** (2008) 701518
5. Baudoz, P., et al., *IAU Colloq. 200*, (2006) 553
6. Galicher, R., et al., *Astronomy and Astrophysics*, **488**, (2008) L9
7. Baudoz, P., et al., *SPIE*, **7736** (2010) 77365S
8. Rouan, D., et al., *PASP*, **112**, (2000) 1479
9. Abe, L., et al., *Astronomy and Astrophysics*, **400**, (2003) 385
10. Galicher, R., et al., *Astronomy and Astrophysics*, **509**, (2010) id.A31
11. Mas, M., et al., *SPIE*, **7735** (2010) 773566
12. Thomas, S., et al., *Applied Optics*, **48** (2009) 4077
13. Borde, P. & Traub, W., *Astrophysical Journal*, **638** (2006) 488